Proc. Natl. Acad. Sci. USA
Vol. 93, pp. 9527–9532, September 1996
Biophysics

The entry and clearance of Ca^{2+} at individual presynaptic active zones of hair cells from the bullfrog's sacculus

(auditory system/Ca^{2+} buffer/confocal microscopy/fluo-3/presynaptic Ca^{2+})

NAOUM P. ISSA* AND A. J. HUDSPETH†

Howard Hughes Medical Institute and Laboratory of Sensory Neuroscience, The Rockefeller University, Box 314, 1230 York Avenue, New York, NY 10021-6399

Contributed by A. J. Hudspeth, June 28, 1996

ABSTRACT **Neurotransmitter is released when Ca^{2+} triggers the fusion of synaptic vesicles with the plasmalemma. To study factors that regulate Ca^{2+} concentration at the presynaptic active zones of hair cells, we used laser-scanning confocal microscopy with the fluorescent Ca^{2+} indicator fluo-3. The experimental results were compared with the predictions of a model of presynaptic Ca^{2+} concentration in which Ca^{2+} enters a cell through a point source, diffuses from the entry site, and binds to fixed or mobile Ca^{2+} buffers. The observed time course and magnitude of fluorescence changes under a variety of conditions were well fit when the model included mobile molecules as the only Ca^{2+} buffer. The results confirm the localized entry of Ca^{2+} underlying neurotransmitter release and suggest that Ca^{2+} is cleared from an active zone almost exclusively by mobile buffer.**

The release of neurotransmitter is initiated by an increase in cytoplasmic Ca^{2+} concentration that occurs when a presynaptic cell is depolarized. Ca^{2+} enters the cell through voltage-activated channels and binds to a Ca^{2+}-sensing protein associated with synaptic vesicles (for review, see ref. 1). This Ca^{2+} sensor is part of a molecular complex that promotes vesicle fusion with the presynaptic membrane. The rate of exocytosis is strongly dependent on the Ca^{2+} concentration at the sensor: Ca^{2+} binding leads to vesicle fusion in a cooperative manner, with a Hill coefficient of 4 at most synapses (2).

Significant progress has been made in elucidating the role of Ca^{2+} as a trigger for neurotransmitter release. The use of fluorescent Ca^{2+} indicators has shown that Ca^{2+} entry is localized to small regions of the cell (3–7); at least in the frog's hair cell, these regions correspond to presynaptic active zones (5). Theoretical analysis suggests that, in less than a millisecond, depolarization elevates the Ca^{2+} concentration immediately adjacent to the presynaptic membrane into the range of hundreds of micromolar (8–13). Indirect measurements, based upon the activation of Ca^{2+}-sensitive channels and competition for Ca^{2+} binding with exogenous buffer, support this inference (14, 15). With such an elevated local Ca^{2+} concentration, efficient triggering of exocytosis does not require that the synaptic vesicle's Ca^{2+} sensor have a high affinity for Ca^{2+}; in fact, the sensor in retinal bipolar cells has a dissociation constant for Ca^{2+} of $\approx$200 μM (16).

Although the prevalent view of transmitter release depends upon the attainment of a high, localized Ca^{2+} concentration at the Ca^{2+}-sensing site of a docked synaptic vesicle, it has not heretofore been possible to test this hypothesis by measuring changes in Ca^{2+} concentration within tens of nanometers of the plasmalemma, where the Ca^{2+} sensors reside. By taking advantage of the structural simplicity of the afferent synapse from the hair cell, the internal ear's sensory receptor, we have measured changes in Ca^{2+} concentration only 50–450 nm from the presynaptic membrane. By comparing our results with the predictions of a model for localized Ca^{2+} entry, we have defined the factors that regulate the presynaptic Ca^{2+} concentration at this synapse.

The publication costs of this article were defrayed in part by page charge payment. This article must therefore be hereby marked "*advertisement*" in accordance with 18 U.S.C. §1734 solely to indicate this fact.

MATERIALS AND METHODS

Methods. Hair cells were isolated from the sacculus of the bullfrog (*Rana catesbeiana*) by a published method (17). Cells were bathed in a standard saline solution containing 110 mM Na^+, 2 mM K^+, 4 mM Ca^{2+}, 118 mM Cl^-, 3 mM D-glucose, and 5 mM Hepes at pH 7.3. Whole-cell voltage-clamp recording was conducted with a patch-clamp amplifier (EPC-7; List Electronics, Darmstadt, Germany) controlled by a computer through an experimental interface (LM-900; Dagan Instruments, Minneapolis). Recording pipettes had resistances of 3–5 MΩ when filled with internal solution containing 200 μM $(NH_4^+)_5$fluo-3, 104 mM Cs^+, 2 mM Na^+, 2 mM Mg^{2+}, 104 mM Cl^-, 1 mM ATP, 5 mM Hepes at pH 7.3, and bis(2-aminophenoxy)ethane-*N*,*N*,*N*′,*N*′-tetra-acetate (BAPTA) or EGTA as specified for each experiment. Cellular currents were filtered with an 8-pole Bessel filter with a corner frequency set at one-quarter the sampling frequency; their linear components were subtracted with a P/6 routine. Depolarizations were synchronized to fluorescence signals either by imaging a probe that moved in response to the voltage-command pulse or by sampling the voltage-command signal with a second analog-to-digital converter in the confocal microscope's computer. Images were acquired using a laser-scanning confocal-illumination system (MRC-600; Bio-Rad; ref. 5). Line-scan images were smoothed with a 3 $\times$ 3 mask (1:2:1, 2:8:2, 1:2:1) that introduced a spread in the time domain of less than 0.6 ms.

Buffered-Diffusion Model. The model evaluated here resembled one used previously (13) but was implemented differently. The movement of Ca^{2+} from the presynaptic active zone into the cell body was modeled using a system of difference equations written in QUICKBASIC (Microsoft, Redmond, WA) and evaluated with an IBM-compatible computer. The model included Ca^{2+} entry through a channel cluster represented as a point source, diffusion of free Ca^{2+} in the cytosol, reaction of Ca^{2+} with one or more buffers, and diffusion of these buffers, either free or bound to Ca^{2+}. The cytoplasm was modeled as nested hemispherical shells, centered about the Ca^{2+}-entry site and extending 6 μm into the cytoplasm. The shell nearest the source was 50 nm thick; more distant shells progressively increased in thickness. Two boundary conditions were imposed: 6 μm from the point source, the concentrations of Ca^{2+} and of free and total buffer were fixed at their initial values; no movement across the plasma mem-

Abbreviation: BAPTA, bis(2-aminophenoxy)ethane-*N*,*N*,*N*′,*N*′-tetra-acetate.

*Present address: Medical Scientist Training Program, University of Texas Southwestern Medical Center, Dallas, TX 75235-9117.
†To whom reprint requests should be addressed. e-mail: hudspaj@rockvax.rockefeller.edu.

brane was permitted except for a step Ca^{2+} current into the first shell.

The buffering of Ca^{2+} was described with a one-step kinetic scheme; all interactions extraneous to rate-limiting Ca^{2+} binding were disregarded. The values of the rate constants and diffusion constant for BAPTA were assumed to be identical to those for fluo-3. We additionally assumed the diffusion constants of free buffers to differ negligibly from those of Ca^{2+}-bound buffers.

The model was iteratively evaluated at time increments of 100 ns; this step size was determined by checking that all solutions were stable and that the use of smaller increments did not significantly alter the results. The model's parameter values were initially selected to reflect the behavior of the chemical species *in vitro*, and subsequently refined by comparison to fluorescence data. Unless otherwise noted, the diffusion constant of free Ca^{2+} was taken as 60×10^{-11} $m^2 \cdot s^{-1}$ (18) and that of fluo-3 as 4×10^{-11} $m^2 \cdot s^{-1}$; the indicator's *on* rate constant was set at 1.39×10^9 $s^{-1} \cdot M^{-1}$ and its *off* rate constant at 550 s^{-1}.

RESULTS

Measurement of the Presynaptic Ca^{2+} Concentration. Individual active zones were identified in frog saccular hair cells loaded with the Ca^{2+} indicator fluo-3. This compound binds reversibly to presynaptic dense bodies (17), active-zone structures found in cells that release neurotransmitter in response to graded changes in membrane potential. In the frog's hair cell, each dense body is a fibrillar sphere, about 400 nm in diameter and lacking a membrane, identifiable in living cells by differential-interference-contrast microscopy (5). Because the dense body is situated within 50 nm of the presynaptic membrane (14, 19), the fluorescence of fluo-3 in this structure provides a readily calibrated measure of the Ca^{2+} concentration at the active zone (17).

To measure the time course of Ca^{2+} entry with high temporal resolution, we used the line-scan feature of a laser-scanning confocal microscope. In this protocol, a 400-nm-wide transect across an isolated hair cell loaded with 200 μM fluo-3 was repeatedly scanned to create a two-dimensional image in which one axis was distance, the other time (Fig. 1*D*). The brightness of each pixel in this image therefore represented the fluorescence intensity of the Ca^{2+} indicator at a particular position and time. To ensure that the transect intercepted a presynaptic active zone, we simultaneously imaged the cell using differential-interference-contrast (Fig. 1*A*) and epifluorescence optics (Fig. 1*B*). Fluo-3 characteristically labeled several presynaptic dense bodies located at the cellular periphery (5, 17). While a line-scan image was being acquired, the membrane was depolarized, eliciting an inward Ca^{2+} current (Fig. 1*C*). Recorded as an increase in fluo-3 fluorescence, the resulting rise in the concentration of free intracellular Ca^{2+} could be calibrated by exposure of synaptic bodies to indicator-saturating Ca^{2+} concentrations (17).

Spatial Profile of Ca^{2+} Concentration. The spatial extent of the increase in free Ca^{2+} concentration depended on the

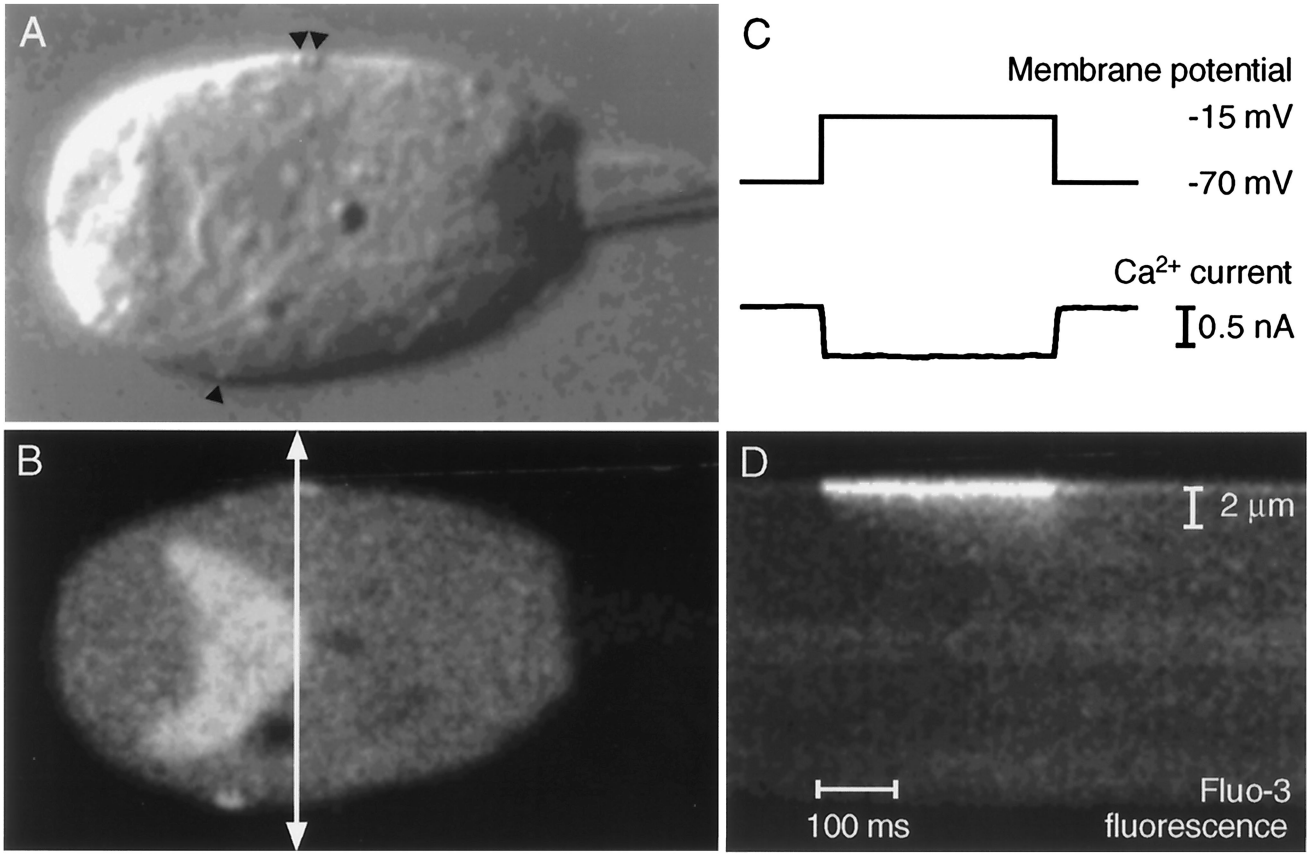

FIG. 1. Experimental protocol. (*A*) In a differential-interference-contrast light micrograph of an isolated hair cell, three of the four presynaptic dense bodies in this plane of focus are visible as round, refractile structures attached to the inner surface of the presynaptic membrane (arrowheads). (*B*) Acquired simultaneously with the image in *A*, a confocal fluorescence image shows that fluo-3 labels the four presynaptic dense bodies. The line with the double arrowhead represents the transect scanned in *D*. (*C*) During the course of imaging, the cell was depolarized for 300 ms from a holding potential of -70 mV to -15 mV (upper trace). This stimulus elicited a sustained whole-cell Ca^{2+} current (lower trace). Because there are $\approx$20 active zones per cell (5, 14, 17), the Ca^{2+} current at a single active zone was $\approx$5% of the whole-cell current. (*D*) A confocal line-scan image was produced by scanning the transect delineated in *B* every 2 ms for a period including the depolarization shown in *C*. During the Ca^{2+} influx, the fluo-3 fluorescence at the active zone first increased rapidly adjacent to the membrane, then gradually rose further away. (The spatial scale bar in *D* also applies to *A* and *B*; the temporal calibration in *D* also applies to *C*.)

duration of Ca^{2+} influx. By the end of a prolonged depolarization, the Ca^{2+} concentration rose throughout the cytoplasm (5, 7). Within a few milliseconds of a depolarization's onset, however, the concentration change was restricted to the region of the cell immediately adjacent to the presynaptic membrane (Fig. 1*D*). This spread demarcated the subdomain of the cell affected by increases in Ca^{2+} concentration during physiological stimulation of fast synapses, whose activation lasts approximately 1 ms (20).

To analyze Ca^{2+} homeostasis in a cell, it is essential to demonstrate the source of diffusing Ca^{2+}. The release of Ca^{2+} from internal stores is apparently not prominent in hair cells (7). Moreover, our earlier study (5) demonstrated that the fluorescence increase at an active zone depends upon Ca^{2+} influx from the bathing medium. In corroboration of this result, we additionally observed a close correlation between Ca^{2+} current and fluorescence at presynaptic active zones. While an indicator-loaded cell was depolarized to various degrees, the Ca^{2+} current and fluorescence change at a presynaptic dense body were recorded (Fig. 2*A*). Comparison of the relation between fluorescence change and membrane potential with a graph of current versus membrane potential revealed that presynaptic Ca^{2+} concentration varied directly with whole-cell Ca^{2+} current (Fig. 2*B*).

Because neurotransmitter release is critically dependent upon the Ca^{2+} concentration at the presynaptic membrane, we investigated the factors regulating this local concentration. The Ca^{2+} pump acts too slowly to affect the presynaptic Ca^{2+} concentration during a brief, physiologically relevant stimulus; this ion pump instead returns the concentration to its resting level over several seconds after the imposition of a Ca^{2+} load (7). By contrast, Ca^{2+} buffer would be expected to effectively attenuate the change in the presynaptic free Ca^{2+} concentration (15, 21). Because fixed buffer might eventually be saturated by Ca^{2+} influx, such a buffer would not necessarily affect the steady-state Ca^{2+} concentration near an entry site (13). If fixed buffer were highly concentrated in presynaptic dense bodies, however, it might attenuate the brief increase in Ca^{2+} concentration associated with physiological stimuli. To examine these possibilities, we quantified the influences of both mobile and fixed buffers on the Ca^{2+} concentration at presynaptic active zones.

Effect of Mobile Buffer. To determine the effect of mobile Ca^{2+} buffer on the time course of changes in presynaptic Ca^{2+} concentration, we loaded hair cells with different concentrations of exogenous buffer and measured the change in local Ca^{2+} concentration during depolarization. In general, high concentrations of mobile buffer limited the spread of Ca^{2+} from the entry site and attenuated the change in local Ca^{2+} concentration (Fig. 3). In the absence of any mobile buffer save fluo-3, a detectable concentration of free Ca^{2+} reached the cell's center within 100 ms. At the opposite extreme, 10 mM BAPTA essentially restricted the increase in free Ca^{2+} concentration to the presynaptic dense body.

The effect of exogenous mobile buffer in attenuating the fluo-3 fluorescence signal was determined by measuring the change in presynaptic fluorescence intensity associated with different Ca^{2+} currents. With increasing concentrations of exogenous buffer, the fluorescence intensity became less sensitive to the Ca^{2+} current. Fig. 4 shows the change in concentration of Ca^{2+}-bound fluo-3 at the presynaptic dense body as a function of whole-cell Ca^{2+} current with four different intracellular concentrations of BAPTA. In a weakly buffering environment (Fig. 4*A*), 200 μM fluo-3 became saturated during large Ca^{2+} influxes. In a strongly buffering environment, however, the indicator was not saturated: the change in fluorescence remained directly proportional to the current (Fig. 4 *B–D*). The slope of the relation between change in fluorescence and Ca^{2+} current decreased with increasing buffer concentration, approaching zero for the highest concentration. Because of the high concentration of mobile Ca^{2+} buffer in an intact hair cell (21), the normal physiological response would likely resemble that in the presence of 3 mM BAPTA.

The most important test of a quantitative model of presynaptic Ca^{2+} dynamics is that it accurately predict the Ca^{2+} concentration near the presynaptic membrane. Without the need to invoke any fixed Ca^{2+} buffer, the localized Ca^{2+}-entry model successfully fit the change in presynaptic fluo-3 fluorescence in response to Ca^{2+} current at several exogenous buffer concentrations (Fig. 4). The model additionally predicted the slope of the fluorescence signal as a function of current and the saturation point of fluo-3 fluorescence as functions of Ca^{2+} current. The agreement of the model with the data provides direct, quantitative confirmation of the

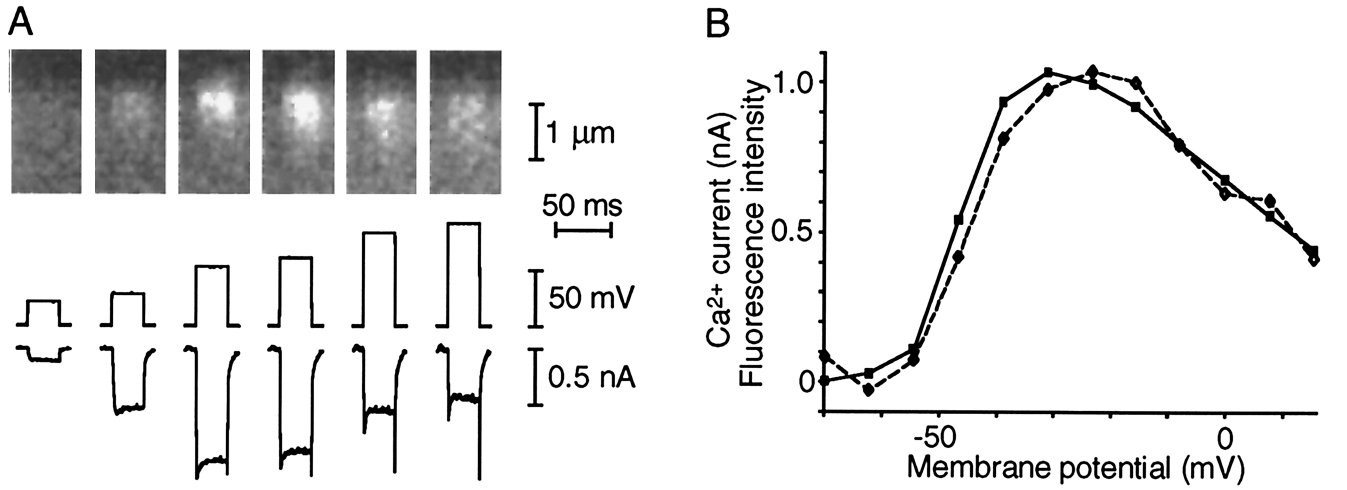

FIG. 2. Linear dependence of presynaptic Ca^{2+} concentration on Ca^{2+} current. (*A*) The fluo-3 fluorescence intensity in the dense body depended on the magnitude of the Ca^{2+} current. While a transect through a presynaptic active zone was scanned (*Top*), the cell was depolarized from a holding potential of −70 mV to six different levels (*Middle*). The magnitude of the whole-cell Ca^{2+} current depended on the extent of depolarization (*Bottom*). The transients at the ends of some traces represent Ca^{2+} tail currents. (*B*) The change in fluorescence intensity (dotted line) during a depolarizing pulse had the same dependence on membrane potential as the Ca^{2+} current (solid line). As long as the indicator did not become saturated with Ca^{2+}, the change in fluo-3 fluorescence was linearly proportional to the whole-cell Ca^{2+} current. The fluorescence signal was normalized to the maximal average value.

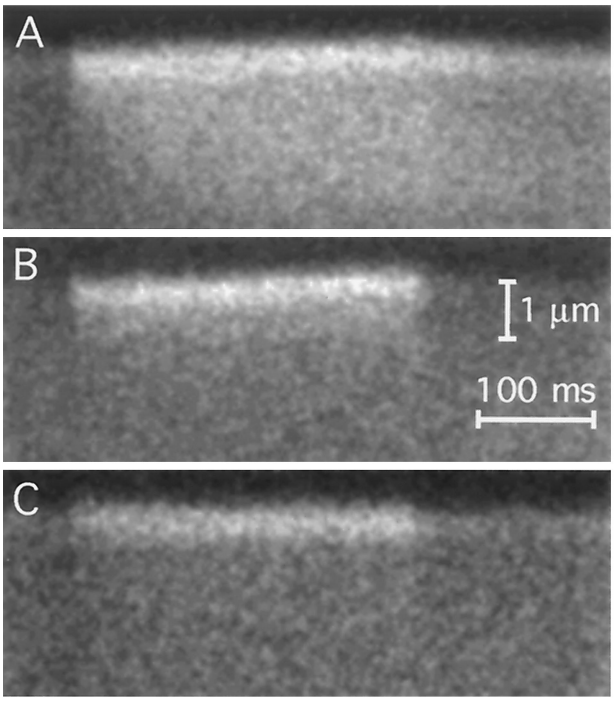

FIG. 3. The effect of exogenous mobile buffer upon the change in fluo-3 fluorescence intensity in response to Ca^{2+} current. During recordings from three different cells, the spatial extent of fluo-3 fluorescence was progressively restricted by inclusion in the recording pipettes of increasing concentrations of buffer (*A*, 200 μM fluo-3; *B*, 200 μM fluo-3 plus 3 mM BAPTA; *C*, 200 μM fluo-3 plus 10 mM BAPTA). The peak Ca^{2+} currents were 0.9 nA for *A*, 0.7 nA for *B*, and 1.1 nA for *C*.

localized Ca^{2+}-entry hypothesis of presynaptic activation proposed in the mid-1980s (8–12).

Temporal Profile of Ca^{2+} Concentration. The rate of increase in presynaptic free Ca^{2+} concentration determines the delay between presynaptic depolarization and neurotransmitter release. Two processes influence the time course of changes in presynaptic Ca^{2+} concentration: the kinetics of Ca^{2+}-channel gating and the dynamics of Ca^{2+} buffering and diffusion. In a voltage-clamped hair cell depolarized to −15 mV, Ca^{2+} channels open completely in less than 1 ms (22). Because neurotransmission occurs almost immediately upon Ca^{2+} influx (23), the Ca^{2+} concentration at the synaptic vesicle's Ca^{2+} sensor must rise extremely rapidly.

In an attempt to resolve the rapid changes in presynaptic Ca^{2+} concentration that occur at the onset of Ca^{2+} influx, we measured the average fluorescence intensity at dense bodies during the first 30 ms of step depolarizations. The time course of the fluo-3 signal revealed two phases of Ca^{2+}-concentration increase (Fig. 5*A*). The fluorescence intensity increased quickly during the initial 6 ms of a depolarizing pulse; this rapid rise represented the increase in Ca^{2+} concentration in the presynaptic dense body. In the second phase, the fluorescence intensity rose significantly more slowly; this slower phase reflected augmented fluorescence in cytoplasmic regions adjacent to the active zone, including those above and below the plane of focus (17).

Fast though it was, the observed fluorescence increase at the onset of a depolarizing pulse was inevitably delayed by the filtering properties of the detection system. To compensate for this delay, the profile of fluo-3–Ca^{2+} concentration derived from the model was subjected to sampling and filtering similar to those imposed upon the experimental data. The resultant profile closely resembled the experimentally determined profile in the rapidly rising phase (Fig. 5*A*), indicating that the underlying events occurred on a time scale consistent with the model's predictions.

The Ca^{2+} concentration remained elevated after the conclusion of a depolarizing pulse. Fluo-3 fluorescence decreased in the dense body with an approximately exponential time course characterized by an average time constant of 17 ms (Fig. 5*B*). With a low buffer concentration, 200 μM fluo-3, the clearance time constant depended linearly on the magnitude of the Ca^{2+} current (Fig. 5*C*). With buffer concentrations exceeding 3.2 mM, however, the time constant was independent of the Ca^{2+} current's magnitude. The clearance time constants for small Ca^{2+} currents were similar for all buffer concentrations.

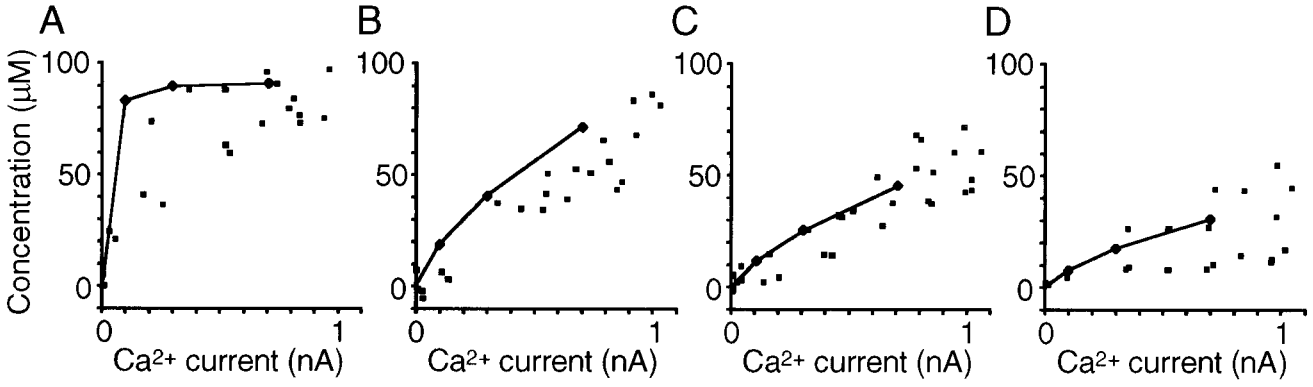

FIG. 4. The role of mobile buffer in attenuating the presynaptic Ca^{2+} concentration. The changes in concentration of Ca^{2+}–fluo-3 complex in the dense body during the first 30 ms of depolarizing pulses (squares) are plotted as functions of the whole-cell Ca^{2+} currents for four concentrations of exogenous mobile Ca^{2+} buffer (*A*, 200 μM fluo-3, two cells, two active zones; *B*, 200 μM fluo-3 plus 3 mM BAPTA, one cell, two active zones; *C*, 200 μM fluo-3 plus 6 mM BAPTA, two cells, two active zones; *D*, 200 μM fluo-3 plus 10 mM BAPTA, one cell, two active zones). Points at which the model was evaluated are shown with diamonds connected by lines. The discrepancy between the data and the model's predictions for the lowest concentration of buffer might have arisen from the presence of fixed buffer or the persistence of some endogenous mobile buffer. Because the fluorescence intensity very near the membrane was attenuated by the lateral resolution of the microscope, the predicted values for the concentration of Ca^{2+}–fluo-3 complex were weighted by the Gaussian function describing the microscope's lateral resolution (17). The cellular boundary was set at the half-height position of the Gaussian curve. In calculating the predicted changes for the instance of 200 μM fluo-3, the total Ca^{2+} concentration was set such that half the indicator was bound to Ca^{2+} at rest, as was the case experimentally; for all other simulations, the total Ca^{2+} concentration was adjusted to give a free Ca^{2+} concentration of 2–3 nM. For estimation of the intracellular Ca^{2+} concentration from fluo-3 fluorescence, the fluorescence intensity of 200 μM fluo-3 saturated with Ca^{2+} was determined from the maximum cytoplasmic intensity attained after extensive cellular depolarization in experiments lacking exogenous Ca^{2+} buffer other the indicator (17).

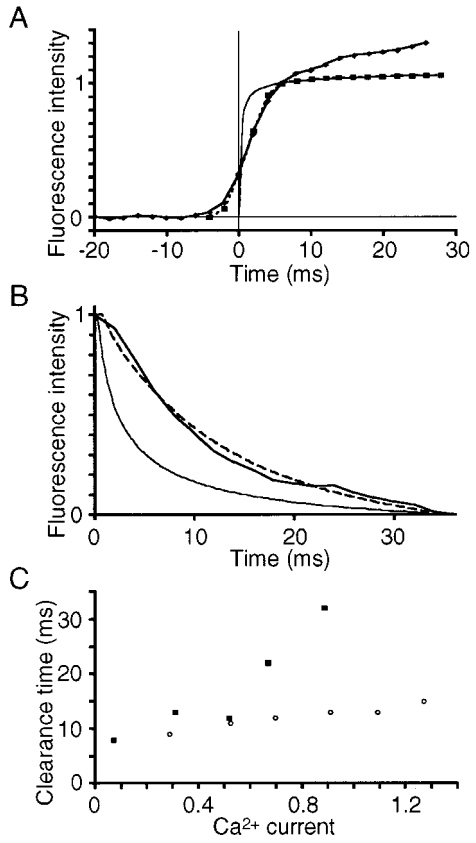

FIG. 5. Temporal profile of fluo-3 fluorescence. (*A*) The average fluorescence profile of fluo-3 in the dense body during the first 26 ms of a depolarizing pulse is shown. The data resulted from 478 depolarizations from 60 cells whose average Ca^{2+} current was 0.6 ± 0.4 nA. The average profile (thick line with diamonds) included data from a variety of buffering conditions: 200 μM fluo-3, 200 μM fluo-3 plus 1 mM, 3 mM, 6 mM, 8 mM, or 10 mM BAPTA, and endogenous cellular buffer, as sampled with the perforated-patch technique (24) and with fluo-3 introduced as its acetoxymethyl ester. Fluorescence intensity was normalized to the value 6 ms after the onset of the depolarizing pulse, at the end of the rapid phase of fluorescence increase. The initial rate of increase in fluorescence did not depend significantly on the concentration of mobile buffer. The slow rising phase in the last third of each trace stemmed from contamination of the fluorescence signal by out-of-focus fluorescence (17). The predicted profile (thin line) had an initial rising phase significantly more abrupt than that of the experimentally measured profile. When the predicted profile was manipulated like the experimental data, however, the resulting profile displayed a rising phase similar to that of the experimentally determined profile (dashed line with squares). The manipulations to the predicted profile included sampling at 2-ms intervals, smoothing with a 1:3:1 moving mask, and averaging with duplicated profiles offset by +2 ms and −2 ms. (*B*) The clearance of fluo-3 fluorescence at the end of the depolarizing pulse is shown for cells loaded with the variety of buffers used in *A*. The experimentally measured fluorescence profile for small Ca^{2+} current magnitudes (thick line) decayed more slowly than the theoretically determined profile in which fluo-3 in the cytoplasm was assigned the same diffusion constant, 12×10^{-11} $m^2 \cdot s^{-1}$, as in water (thin line). If the diffusion constant of fluo-3 in the model was decreased to 4×10^{-11} $m^2 \cdot s^{-1}$, the theoretically determined profile (dashed line) matched the experimental measurement. (*C*) Clearance time as a function of Ca^{2+} current at different buffer concentrations. At a low buffer concentration, 200 μM fluo-3, the fluorescence clearance time at the end of a depolarizing pulse (solid squares) depended upon the degree of buffer saturation, and hence upon the Ca^{2+} current. In contrast, the clearance time (open circles) for a high buffer concentration, 200 μM fluo-3 plus 10 mM BAPTA, was independent of the magnitude of the Ca^{2+} current. For small current magnitudes, the clearance time was approximately equal for all buffer concentrations.

The decline in fluorescence at the end of a depolarizing pulse was significantly slower than predicted for the diffusion of free Ca^{2+}. This result is not surprising: the majority of Ca^{2+} that enters a cell is captured by buffer (13, 25–27). If the local buffer has an adequate capacity and a sufficiently small dissociation constant for Ca^{2+} binding, the majority of the Ca^{2+} should be cleared from the entry site at the buffer's rate of diffusion. In fact, the results of our simulations with different diffusion constants for Ca^{2+} confirmed that the fluorescence and free Ca^{2+} concentration profiles should have been nearly independent of the diffusion constant of Ca^{2+}.

The predicted time course of fluo-3 fluorescence, and in particular the rate of Ca^{2+} clearance at the conclusion of a pulse, should instead have been sensitive to the diffusion constant of fluo-3. The experimentally observed decline in fluorescence was well fit by assuming a cytoplasmic diffusion constant for fluo-3 and BAPTA of 4×10^{-11} $m^2 \cdot s^{-1}$, approximately one-third that measured in solution (Fig. 5*B*). Because transient cytoplasmic binding decreases the mobility of Ca^{2+} chelators structurally similar to fluo-3 (28, 29), this estimate for the indicator's cytoplasmic diffusion constant seems reasonable.

Potential Role of Fixed Ca^{2+} Buffer. An alternative explanation for the prolonged decline of presynaptic fluo-3 fluorescence is that fixed buffer at the active zone, loaded with Ca^{2+} during the depolarizing pulse, releases Ca^{2+} at the pulse's end (13). The effect of a fixed buffer on the fluorescence profile depends upon the buffer's total concentration and upon the dissociation constant for Ca^{2+} of the fixed buffer relative to that of fluo-3. If the local concentration of fixed buffer were small compared with that of mobile buffer, then the fixed buffer would have a negligible effect on the clearance profile. At the end of a current pulse, the fixed buffer would have little bound Ca^{2+} to contribute to the pool of free Ca^{2+}. If the concentration of fixed buffer were to substantially exceed that of fluo-3, however, this buffer would maintain the local free Ca^{2+} concentration and thus create a plateau in the fluo-3 fluorescence profile at the dissociation constant of the fixed buffer.

Three observations suggested that fixed buffer does not play a significant role at the active zone during moderate Ca^{2+} currents. First, no plateau was apparent in the fluorescence-clearance profile. This result indicates that there was not a large amount of fixed buffer at the active zone with a dissociation constant between 100 nM and 100 μM. Second, consistent with the first observation, the local change in fluo-3 fluorescence as a function of Ca^{2+} current was of the magnitude and time course anticipated if exogenous buffer were the only significant Ca^{2+} buffer (Figs. 4 and 5). Finally, for nonsaturating Ca^{2+} currents, the time constant for Ca^{2+} clearance in the presence of 10 mM BAPTA equalled that with lower buffer concentrations (Fig. 5*C*).

The presynaptic dense body is well situated to regulate the presynaptic Ca^{2+} concentration (13). Two findings, however, suggest that the structure has little such effect. Because there appears to be no significant amount of fixed buffer near the active zone, the dense body evidently does not act as a Ca^{2+} sink. Moreover, Ca^{2+} bound to fluo-3 and other mobile buffers progresses rapidly through the dense body, so this structure does not provide a barrier to Ca^{2+} diffusion. If the dense body should prove to bind endogenous buffer as it binds fluo-3 and other substances (17), the structure might serve as a repository for Ca^{2+} buffer; there is no evidence, however, to suggest that this is the case.

DISCUSSION

By providing a consistent picture of the spatial pattern and time course of elevation in the free Ca^{2+} concentration at the presynaptic active zone, the results presented here validate a specific model of localized Ca^{2+} homeostasis involved in neurotransmitter release (13). In particular, our data indicate

that the free Ca^{2+} concentration only 50–450 nm from the Ca^{2+} sensor of the synaptic vesicle is predominantly determined by the activity of mobile Ca^{2+} buffer. The model of Ca^{2+} homeostasis also permits estimation of the concentration even closer to the sensor: the average Ca^{2+} concentration between the plasmalemma and dense body is about 1 mM during a depolarization to −20 mV or roughly 200 μM during a more physiologically relevant depolarization of 5 mV from the resting potential. These values are consistent with the requirement for a relatively high local Ca^{2+} concentration to trigger synaptic-vesicle fusion and neurotransmitter release (16) and with the indirect measurement of Ca^{2+} concentration at the hair cell's presynaptic active zone (14).

The hair cell's functions place extraordinary demands upon its synapses. To mediate the localization of sound sources by measurement of phase differences in the signals reaching the two ears, hair cells must release synaptic transmitter in an oscillatory manner at frequencies approaching 10 kHz (30). To achieve such rates of transmitter release, the Ca^{2+} concentration at sites of vesicle exocytosis must be modulated with a period as short as 100 μs. The exceptional rapidity of activation and deactivation of the hair cell's Ca^{2+} channels (22) helps to meet this specification. Of equal importance, however, is the reduction of the local Ca^{2+} concentration at the end of each cycle of Ca^{2+} channel. As the present results demonstrate, mobile Ca^{2+} buffer is of critical importance in returning the Ca^{2+} concentration toward its resting level and thus reducing the rate of transmittter release. In contrast to its importance in cells whose exocytotic rate is far smaller (31), fixed buffer plays little role in the rapid modulation of Ca^{2+} concentration in hair cells: by retaining Ca^{2+} near its site of entry, fixed buffer might even reduce the rate at which synaptic release could be modulated. For this reason, evolution may have reduced the concentration of fixed Ca^{2+} buffer at the presynaptic active zones of hair cells even as it increased the amount of mobile buffer to an exceptional level.

We thank Drs. D. W. Hilgemann, F. N. Katz, K. Luby-Phelps, and W. M. Roberts, as well as members of our research group, for helpful comments on drafts of the manuscript. Begun at University of Texas Southwestern Medical Center, this research was supported by National Institutes of Health Grant DC00317. A.J.H. is an Investigator of Howard Hughes Medical Institute.

1. Südhof, T. C. (1995) *Nature (London)* **375,** 645–653.
2. Dodge, F. A. & Rahamimoff, R. (1967) *J. Physiol. (London)* **193,** 419–432.
3. Llinas, R., Sugimori, M. & Silver, R. B. (1992) *Science* **256,** 677–679.
4. Callaway, J. C., Lasser-Ross, N., Stuart, A. E. & Ross, W. N. (1993) *J. Neurosci.* **13,** 1157–1166.
5. Issa, N. P. & Hudspeth, A. J. (1994) *Proc. Natl. Acad. Sci. USA* **91,** 7578–7582.
6. Robinson, I. M., Finnegan, J. M., Monck, J. R., Wightman, R. M. & Fernandez, J. (1995) *Proc. Natl. Acad. Sci. USA* **92,** 2474–2478.
7. Tucker, T. & Fettiplace, R. (1995) *Neuron* **15,** 1323–1335.
8. Chad, J. E. & Eckert, R. (1984) *Biophys. J.* **45,** 993–999.
9. Simon, S. M. & Llinas, R. R. (1985) *Biophys. J.* **48,** 485–498.
10. Fogelson, A. L. & Zucker, R. S. (1985) *Biophys. J.* **48,** 1003–1016.
11. Zucker, R. S. & Fogelson, A. L. (1986) *Proc. Natl. Acad. Sci. USA* **83,** 3032–3036.
12. Neher, E. (1986) in *Calcium Electrogenesis and Neuronal Functioning*, eds. Heinemann, U., Klee, M., Neher, E. & Singer, W. (Springer, Berlin), pp. 80–96.
13. Roberts, W. M. (1994) *J. Neurosci.* **14,** 3246–3262.
14. Roberts, W. M., Jacobs, R. A. & Hudspeth, A. J. (1990) *J. Neurosci.* **10,** 3664–3684.
15. Adler, E. M., Augustine, G. J., Duffy, S. N. & Charlton, M. P. (1991) *J. Neurosci.* **11,** 1496–1507.
16. Heidelberger, R., Heinemann, C., Neher, E. & Matthews, G. (1994) *Nature (London)* **371,** 513–515.
17. Issa, N. P. & Hudspeth, A. J. (1996) *J. Neurocytol.* **25,** 257–266.
18. Hodgkin, A. L. & Keynes, R. D. (1957) *J. Physiol. (London)* **138,** 253–281.
19. Jacobs, R. A. & Hudspeth, A. J. (1990) *Cold Spring Harbor Symp. Quant. Biol.* **55,** 547–561.
20. Barrett, E. E. & Stevens, C. F. (1972) *J. Physiol. (London)* **227,** 691–708.
21. Roberts, W. M. (1993) *Nature (London)* **363,** 74–76.
22. Hudspeth, A. J. & Lewis, R. S. (1988) *J. Physiol. (London)* **400,** 237–274.
23. Llinas, R., Steinberg, I. Z. & Walton, K. (1976) *Proc. Natl. Acad. Sci. USA* **73,** 2918–2922.
24. Horn, R. & Marty, A. (1988) *J. Gen. Physiol.* **92,** 145–159.
25. Connor, J. A. & Nikolakopoulou, G. (1982) *Lect. Math. Life Sci.* **15,** 79–101.
26. Sala, F. & Hernandez-Cruz, A. (1990) *Biophys. J.* **57,** 313–324.
27. Nowycky, M. C. & Pinter, M. J. (1993) *Biophys. J.* **64,** 77–91.
28. Baylor, S. M. & Hollingworth, S. (1988) *J. Physiol. (London)* **403,** 151–192.
29. Konishi, M., Hollingworth, S., Harkins, A. B. & Baylor, S. M. (1991) *J. Gen. Physiol.* **97,** 271–301.
30. Sullivan, W. E. & Konishi, M. (1984) *J. Neurosci.* **4,** 1787–1799.
31. Chow, R. H., Klingauf, J., Heinemann, C., Zucker, R. S. & Neher, E. (1996) *Neuron* **16,** 369–376.